A Facile Nitriding Approach for Improved Impact Wear of Martensitic Cold-Work Steel Using H₂/N₂ Mixture Gas in an AC Pulsed Atmospheric Plasma Jet

Jhao-Yu Guo [1] 📷, **Yu-Lin Kuo** [1,2,*] 📷 **and Hsien-Po Wang** [1] 📷

1   Department of Mechanical Engineering, National Taiwan University of Science and Technology, Taipei 106335, Taiwan; D10603008@mail.ntust.edu.tw (J.-Y.G.); m10503524@mail.ntust.edu.tw (H.-P.W.)
2   Center of Automation and Control, National Taiwan University of Science and Technology, Taipei 106335, Taiwan
*   Correspondence: ylkuo@mail.ntust.edu.tw; Tel.: +886-2-27376784; Fax: +886-2-27376460

Abstract: In this study, we propose a rapid plasma-assisted nitriding process using H_2/N_2 mixture gas in an atmospheric pressure plasma jet (APPJ) system to treat the surface of SKD11 cold-working steel in order to increase its surface hardness. The generated NH radicals in the plasma region are used to implement an ion-bombardment for nitriding the tempered martensite structure of SKD11 within 18 min to form the functional nitride layer with an increased microhardness around 1095 $HV_{0.3}$. Higher ratios of H/E and H^3/E^2 were obtained for the values of 4.514×10^{-2} and 2.244×10^{-2}, referring to a higher deformation resistance as compared with the pristine sample. After multi-cycling impact tests, smaller and shallower impact craters with less surface oxidation on plasma-treated SKD11 were distinctly proven to have the higher impact wear resistance. Therefore, the atmospheric pressure plasma nitriding process can enable a rapid thermochemical nitriding process to form a protective layer with unique advantages that increase the deformation-resistance and impact-resistance, improving the lifetime of SKD11 tool steel as die materials.

Keywords: atmospheric pressure plasma jet (APPJ); nitriding; functional nitride layer; cold-working steel; surface hardness; impact wear

1. Introduction

Tool steels are used to make manufacturing tools for metal shaping, cutting, and forming into components and accessories. There are broadly seven classifications of tool steels: water-hardening steels, mold steels, shock-resistant steels, hot-work steels, cold-work steels, high-speed steels, and special purposes steels [1]. SKD11 is a cold-work steel used in molds and dies for applications such as drawing, blanking, and piercing with prepared dies due to its excellent characteristics of wear and abrasion resistance [2]. Though SKD11 has good properties, there is a strong need for the use of dies that exhibit a longer lifetime for the mass production of industrial parts. The service life and damage of dies are essential considerations for performance and economic production. However, dies commonly fail due to wear, chipping, cracking, plastic deformation, and so on. To realize the need for long-life high-precision cold-work dies, several methods have been selected for implementing heat and surface treatments: quench/tempering, high-frequency hardening, laser hardening, carburizing, nitriding, physical vapor deposition (PVD), and chemical vapor deposition (CVD) [3]. Among these, nitriding is a thermochemical surface treatment process that introduces nitrogen (N) into the steel surface for achieving greater surface hardness, wear, fatigue, corrosion resistance, and toughness in the performance of components [4,5]. There are three types of conventional nitriding processes: ion nitriding (plasma nitriding), gas nitriding, and salt bath nitriding. Plasma nitriding is conducted with a glow discharge in H_2 and N_2 mixture gas in a vacuum chamber to a pressure of

100–800 Pa for the batch process, with the part at a temperature between 400 and 800 °C. The positively charged nitrogen ions generated in the plasma system are used to bombard the metal substrate, causing nitrogen to penetrate the surface and diffuse into the part [6]. In the manufacturing industry, the part is heated in dry ammonia gas (NH_3) or N_2/H_2 mixture gas for gas nitriding at temperatures in the range of 450–590 °C [7]. Salt bath nitriding is a process in which the product is immersed in a molten salt bath containing cyanides or cyanates with a temperature of 510–580 °C. The most general composition is 30–40% potassium salts and 60–70% sodium salts [8]. It is obvious that the commonality among the three methods is the need to take many hours treating specimens for nitridation in a vacuum chamber, closed chamber, and salt bath [8,9]. The nitriding process improves impact wear resistance and wear resistance, and a linear relationship has been found between the case depth of steel and impact resistance [10,11]. However, there are few studies on the innovative nitriding processes, even though the nitriding process is extensively used in industry.

Atmospheric pressure plasma jet (APPJ) has been discussed in recent decades as a promising technique in extensive applications. It utilizes plasma at normal pressure, offering possible advantages of eliminating an expensive vacuum system, on-line processing capabilities, high efficiency, and scalability to a larger area [12]. The reported applications, such as biological responses, surface modifications of polymers, etching, film deposition, and agriculture, have been widely discussed [13]. As mentioned above, we are developing a plasma nitriding process that is used in atmospheric pressure. In recent years, many researchers have succeeded in using dielectric barrier discharge, microwave-induced nitrogen plasma, and pulsed-arc plasma jet on steel, reaching surface modification under atmospheric pressure [14–16]. To date, much is known about the nitriding processes on tool steels, which is essential for the formation of an excellent surface-hardening layer. Therefore, we propose a facile thermochemical process using H_2/N_2 working gas in an APPJ system for hardening SKD11 cold-work steel to alter its impact wear behavior as mold materials.

2. Experimental Details

2.1. Materials

SKD11 cold-work tool steel was first cut into 15 mm × 15 mm × 6 mm (length × width × height) samples of which the chemical composition is reported in Table 1. These samples were austenitized at 1030 °C for 1 h, quenched in oil, and then double tempered at 550 °C for 2 h. The materials reached the value of hardness around 558 ± 5.9 $HV_{0.3}$ (HRC 55). After the heat treatment process, all specimens were ground and mechanically polished, forming a mirror-like surface. Finally, specimens were cleaned and degraded ultrasonically in acetone prior to the plasma process.

Table 1. Chemical composition (wt.%) of SKD11 cold-work steel.

Fe	Cr	C	Mo	Si	Mn	V	Co	P	S
Bal.	11.2	1.68–1.41	0.53	0.34	0.30	0.191	0.06	0.02	0.006

2.2. APPJ System

We used a commercial APPJ system (Click-SSV1, Click Sun-Shine Corp., New Taipei City, Taiwan) with a fixed-jet nozzle for treating the SKD11 samples, as depicted in Figure 1. The sample was set on the substrate holder with the sample-to-nozzle distance of 3 mm. The substrate holder was neither heated nor cooled. The plasma jet was equipped with a quartz tube in order to prevent surface oxidation by air from the ambient environment and maintain the plasma-induced temperature on the sample surface during the nitriding process. For use of the hydrogen gas at atmospheric pressure, however, the lower limit concentration of hydrogen gas to form an explosive mixture with the air (around 4.0%) was seriously considered [17]. During the surface treatment, the AC-pulse power supplied

to the plasma discharge was kept at 500 W, and the flow rate of 2% H_2/98% N_2 (vol%) mixture as working gas was maintained at 35 slm by the mass flow controller. In order to realize the plasma species generated by the 2% H_2/N_2 mixture gas in an APPJ system, an optical fiber sensor near the plasma was placed, as shown in Figure 1. The optical emission spectroscopy (OES) was measured using a Mars HS2000+ (GIE Optoelectronics Inc., Taipei, Taiwan) with wavelengths from 200 nm to 900 nm for plasma species diagnosis.
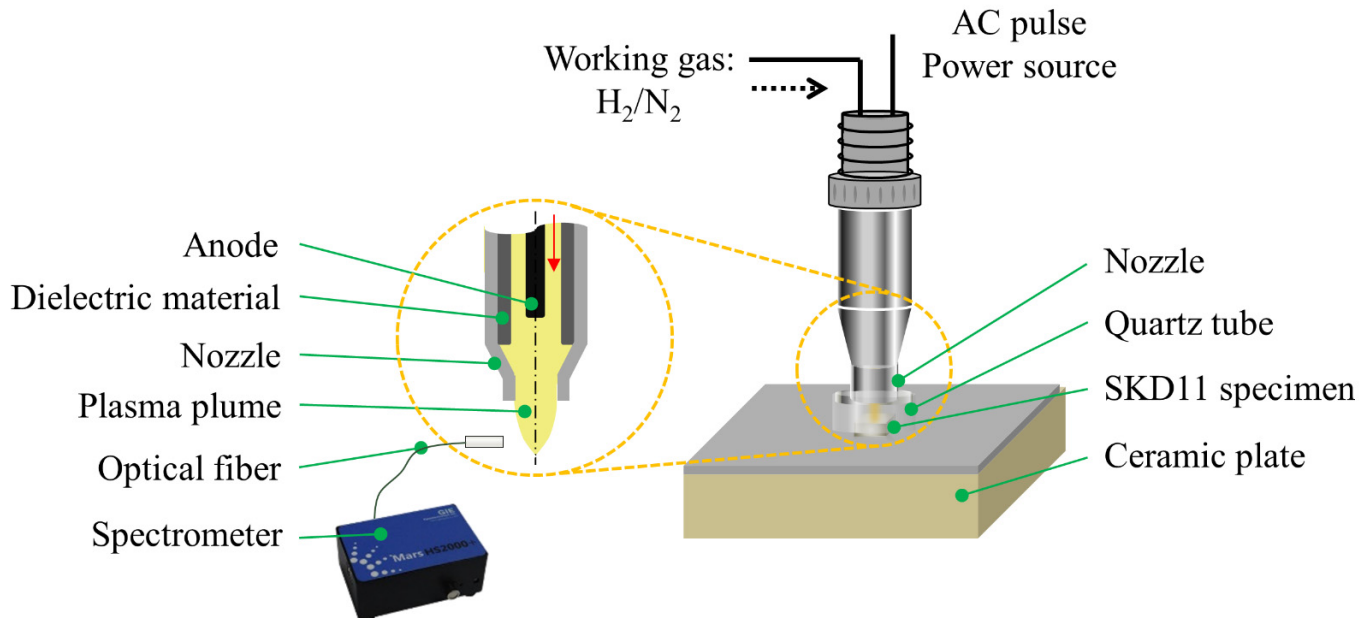

Figure 1. Schematic set-up of the APPJ system for the nitriding process.

The most important factor of the nitriding process is the reaction temperature control. Furthermore, a nitriding process is necessarily required for suitable treatment temperature range from 260 °C to 600 °C [18]. We employed the atmospheric pressure plasma nitriding (APPN) process to offer high energetic plasma species, which were used to bombard the substrate and inherently induce the heat to reach a stable temperature. The substrate temperature was monitored using a thermometer (TES-1370, TES Electrical Electronic Corp., Taipei, Taiwan) with a thermocouple covered with a quartz pipe placed inside the samples to monitor the process. After holding the plasma exposure in the APPN process for 10 min, the plasma system was turned off to allow the sample to cool down with nitrogen gas flow to reach room temperature, as shown in Figure 2a. For the accurate measurement of the temperature profile on substrates, the temperature gradient induced by plasma bombardment on the sample of SKD11 cold-work steel at different locations was proposed for the measurement, as shown in Figure 2b. However, the temperature evolution on the top point (surface) could not be measured accurately due to the electrons of the plasma attacking the thermocouple and causing the thermometer to be disabled. Furthermore, the temperatures at the bottom and the middle point of the substrate were obtained at stable values of approximately 500 °C and 535 °C, respectively, inferring that the substrate surface possesses a higher temperature than 535 °C.

2.3. Materials' Characterization

After the APPJ treatment, an X-ray diffractometer (XRD, D2-phaser X-ray diffraction, Bruker, Billerica, MA, USA) with Cu Kα (λ = 1.5406 Å) radiation was used to observe the phases formed near the surface. Chemical compositions of samples were investigated by X-ray photoelectron spectroscopy (XPS) measurements performed using a Theta Probe electron spectrometer (Thermo Fisher Scientific Inc., East Grinstead, UK) with a monochromated anode Al Kα (hν = 1486.6 eV) source operated at 15 kV. Peak positions were then

energy scale calibrated with respect to the C1s peak at 284.5 eV from the adventitious hydrocarbon beneficial contamination.
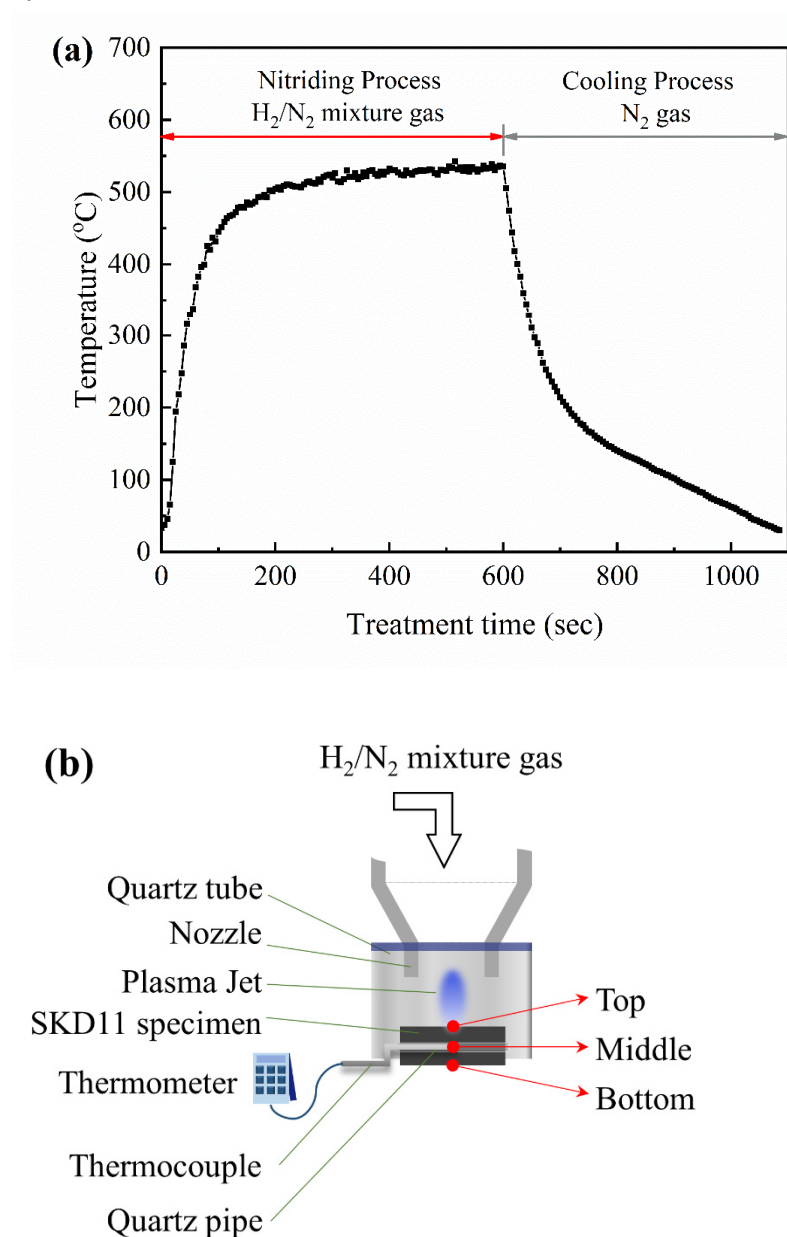

Figure 2. (**a**) Integrated treatment cycle of the APPJ system for the nitriding process. (**b**) Schematic setup for temperature measurements during the nitriding process on SKD11 steel specimen.

　　　Surface hardness measurements were carried out for untreated and treated specimens using a Vickers indenter (HV, MVK-H1, Mitutoyo Inc., Kanagawa, Japan) at a constant load of 0.3 kg and loading time of 15 s. The microstructures of the base material and the treated specimens polished and etched in 5% Nital solution were investigated metallographically by applying a Zeiss Axio Lab A1 optical microscope (OM, Leader Inc., New Taipei City, Taiwan). Field emission scanning electron microscopy (FESEM, 7900 type, JEOL, Tokyo, Japan) was used to analyze the cross-sectional morphology and the nitrogen content of the treated surface. The mechanical properties of nanohardness (H) and elastic modulus (E) for the plasma-treated SKD11 sample were obtained by a nanoindenter (Hysitron TI-980 nanoindenter, Bruker, Minneapolis, MN, USA) using a Berkovich 142.3° diamond probe.

　　　In this test, the indent probe came into contact with the sample surface, gave force into the material, and then left the sample. The data for load (*P*), displacement (*h*), and time (*t*)

were recorded. The equation connecting the reduced Young's modulus (E_r) and Young's modulus (E) of the sample and the indenter was set up by Oliver and Pharr, which is described as follows [19]:

$$\frac{1}{E_r} = \frac{(1 - v_s^2)}{E} + \frac{(1 - v_{ind}^2)}{E_{ind}} \tag{1}$$

where E_{ind} and v_{ind} are Young's modulus (1140 GPa) and Poisson's ratio (0.07) for the Berkovich diamond indenter, respectively [19]. For the impact wear testing, the frequency, impact force, and impact ball to sample distance were set at values of 20 Hz, 9.8 N, and 1 cm, respectively. Multi-cycling impacts using a tungsten carbide ball were applied to observe the impact point for understanding the plastic deformation [20].

3. Results and Discussion

The sufficient treatment temperature generated on the sample surface and the H_2/N_2 mixture as plasma nitriding gases in an APPJ system were prepared, which are necessarily required for the plasma nitriding processes. To understand the nitriding behavior of the SKD11 sample by the APPN process, we first performed XRD analysis to investigate the structural variation and nitride formation of the treated surface. The pristine SKD11 sample mainly possesses a martensitic microstructure, identifying the present metals of α-Fe at 2θ = 44.5°, 64.64°, and 81.92° for ferrite; γ phase at 2θ = 43.54°, 50.55°, and 74.55°; and (Fe, Cr)$_7$C$_3$ at 2θ = 39.42° and 52.44° for iron-chromium carbide, as shown in Figure 3a [21–23]. For the APPN-treated SKD11 samples, Figure 3b displays the formation of two types of iron nitride, γ'-Fe$_4$N (2θ positions of 41.65°, 48.16°, and 70.12°) and ε-Fe$_{2\text{-}3}$N (2θ positions of 38.96°, 41.65°, 44.4°, 58.08°, 70.12°, 77.4°, and 84.7°), carlsbergite (2θ positions of 37.84° and 63.72° for CrN) [24–26]. As a result, the APPN method in this research could succeed in the formation of the nitriding layer of γ'-Fe$_4$N and ε-Fe$_{2\text{-}3}$N, and it is consistent with other traditional nitriding processes [27,28].
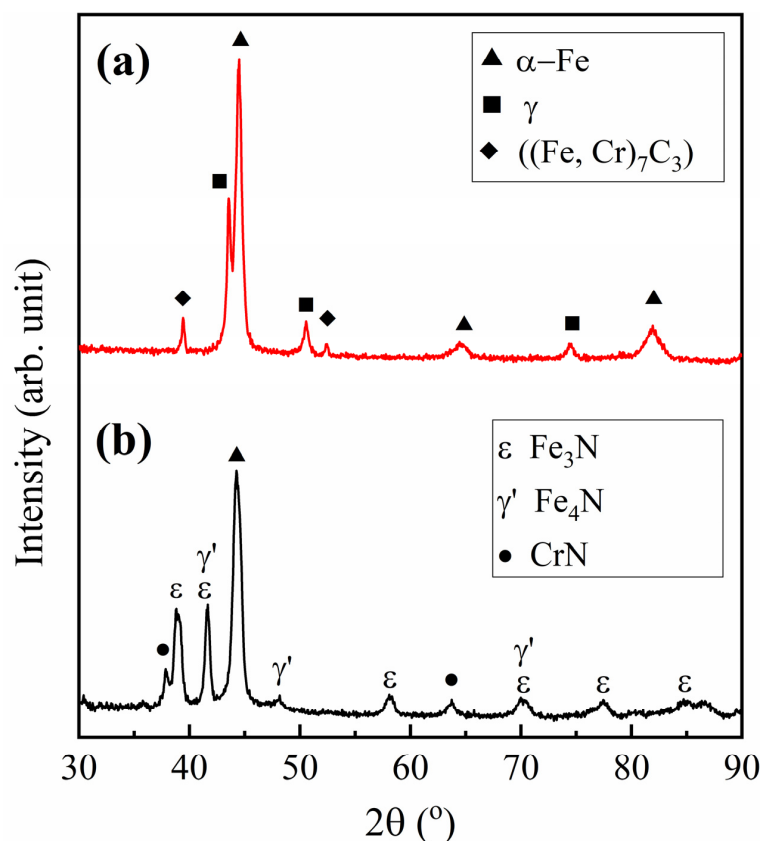

Figure 3. XRD results of (**a**) pristine SKD11 and (**b**) APPN-treated SKD11 samples.

Figure 4 represents a wide range from 0 to 1300 eV by XPS analyses for the pristine SKD11 specimen and the APPN-treated SKD11 specimen. All XPS binding energies of Fe, Cr, C, and O photoelectrons for pristine SKD11 are consistent with the database from the XPS handbook [29]. For the APPN-treated SKD11 specimen, however, the peak intensity of O1s located around 530 eV decreased. This may be due to the involved reduction of metal oxide on the surface originally required for the nitridation process using H_2/N_2 mixture gases [30].
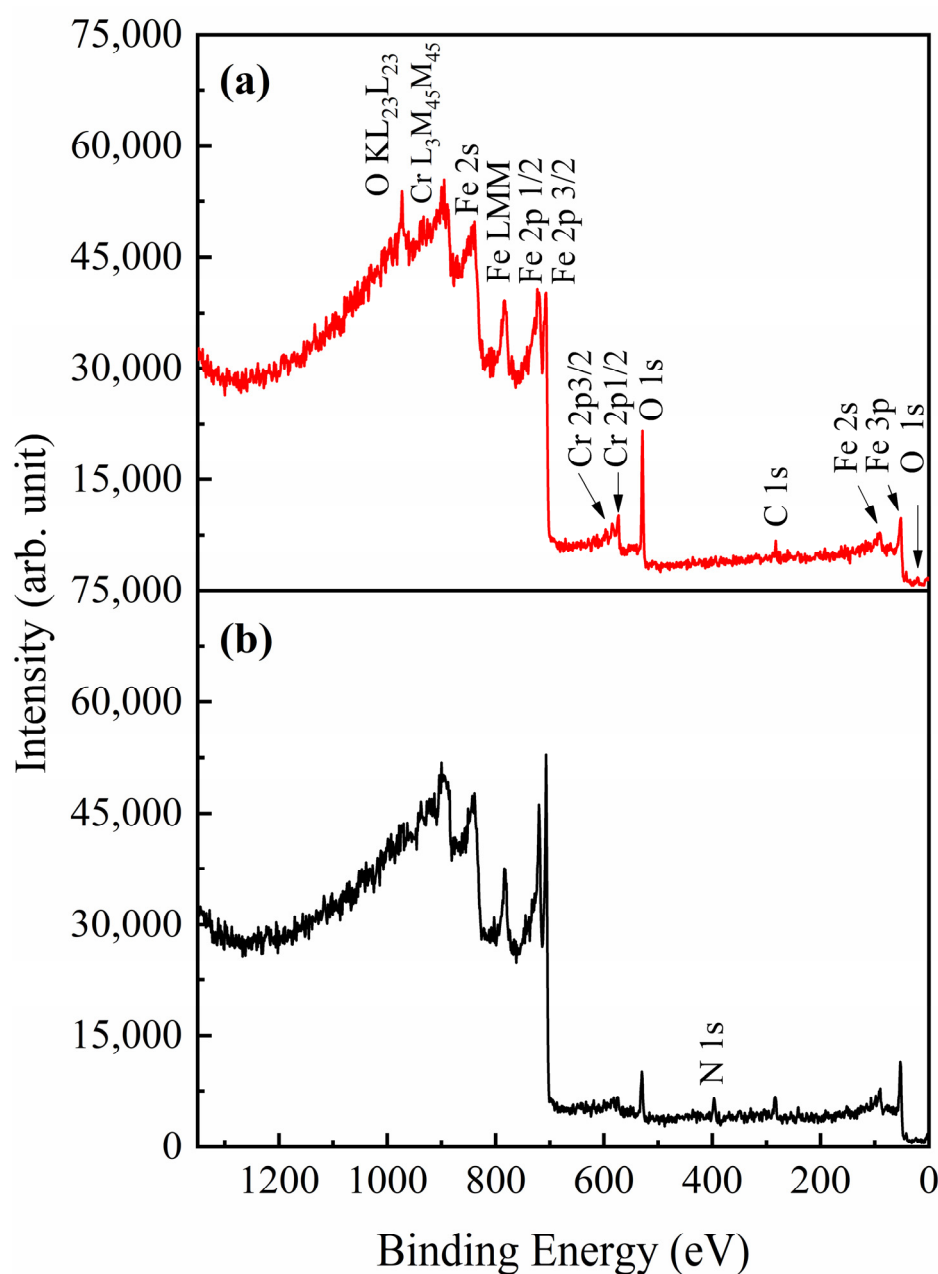

Figure 4. Wide scans of XPS analyses of (**a**) pristine SKD11 and (**b**) APPN-treated SKD11 samples.

Based on the arguments mentioned above, the results of the XPS spectrum with the additional N1s peak at 397 eV could be clearly observed, inferring that the nitrogen element diffused into the substrate to combine with the metal matrix for the formation of metal nitrides [31]. The nitriding process on steels generally produces modified surface layers, the characteristics of which depend on the process parameters and the substrate conditions [8]. The results of XRD and XPS indicate that the modified surface layers on SKD11

by the APPN process mainly consisted of γ'-Fe_4N, ε-$Fe_{2-3}N$, and CrN, confirming the evidence of nitrogen atoms reacting with the metal elements under the plasma-induced surface temperature above 535 °C.

Figure 5a reveals the OM image for the cross-sectional microstructure of the APPN-treated sample. Three clear zones from the cross-sectional image represent three different parts. The bottom region is the base material (B.M.), in which the microstructure is the tempered martensite [32]. The compound zone (C.Z.) contributed by the nitride formation on the top surface is a white layer with a thickness of around 12.5 μm, while the dark region below the white layer is recognized as the diffusion zone (D.Z.) with a thickness of around 31.5 μm [8,33]. The principle of the nitride formation is through nucleation and continues until consecutive nucleation of iron nitride on the metallic surface. The atomic radius of iron is greater than nitrogen (N: 0.72 Å, Fe: 1.28 Å). As mentioned above, the nitrogen element is allowed to enter the α-iron crystal structure as the interstitial solute atom. On the other hand, the solubility rate of the nitrogen atom at 400–600 °C is definitely greater than at 20 °C in ferrite, because the high temperature process leads to elongate lattice constants [33]. Therefore, the compound layer consists of γ'-Fe_4N, ε-$Fe_{2-3}N$, and other alloying elements, while the diffusion zone consists mainly of nitrogen atoms dissolved, alloying elements in the form of solid solution, and dispersed fine nitrides in the metal.
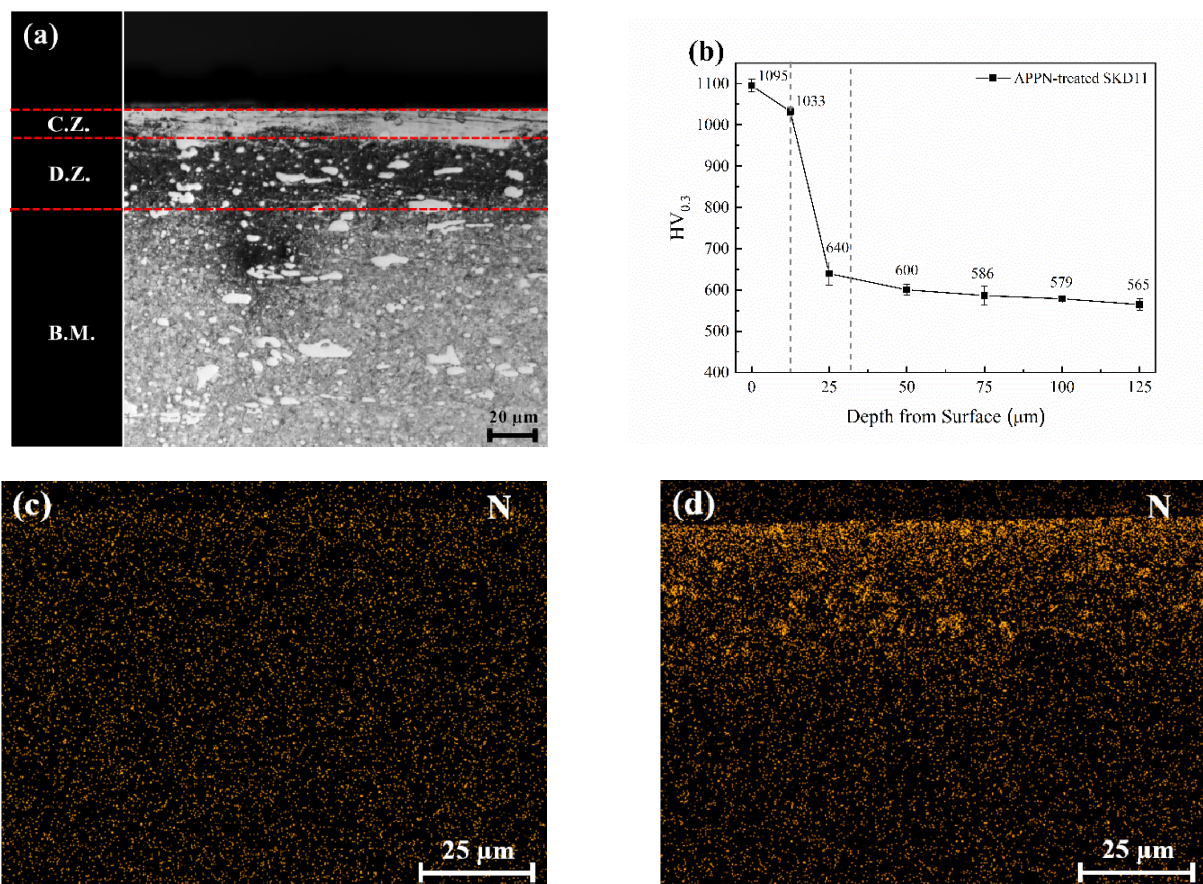

Figure 5. Materials' characterizations of the samples: (**a**) cross-sectional optical microscope image of APPN-treated SKD11, (**b**) the hardness depth profile of APPN-treated SKD11, and EDS nitrogen mapping of (**c**) pristine SKD11, and (**d**) APPN-treated SKD11.

The microhardness of the pristine SKD11 sample, as a result of the tempered martensite structure formed after the heat pretreatment process, is approximately 558 ± 5.9 $HV_{0.3}$. The microhardness depth profile of the APPN-treated SKD11 sample appears in Figure 5b. The modified surface layers on the SKD11 sample reached a higher value of 1095 ± 15.5 $HV_{0.3}$

at its top point, which is harder than the pristine SKD11. The higher microhardness value of alloy steel for an appropriate nitriding temperature is due to the alloying elements forming stable nitrides [34]. The covalent bond of stable nitrides has a bond energy that is much higher than the metallic bond of steel. Thus, the value in the compound zone within the nitride layer is nearly constant. However, into the diffusion zone, the microhardness gradually decreased to the matrix value.

The microhardness depth profile also corresponds with the thickness values of the compound layer and diffusion layer estimated from the OM image in Figure 5a. The energy dispersive spectroscopy (EDS) for nitrogen elemental mapping analyses of the pristine SKD11 and APPN-treated SKD11 samples is shown in Figure 5c,d, respectively. It is observed that the nitrogen content of pristine SKD11 was not clear, confirming nitrogen-free atom cumulative on SKD11 steel. In Figure 5d, the compound layer contributed by the nitrides formed on the top surface of APPN-treated SKD11 displays a nitrogen-rich surface and then displays a sudden decrease in nitrogen content to the core transition.

To gain further insight into the mechanism of nitriding on SKD11 cold-work steel and to identify the reactive plasma species involved in the 2% H_2/N_2 plasma exposure in the APPJ system, plasma diagnosis was applied by OES. In Figure 6a, the spectral characteristics between 200 and 900 nm from 2% H_2/N_2 plasma exposure were identified using NIST reference data [35]. Figure 6b shows that the results of the obtained emission intensities for NH (336 nm), N_2 (295.3 nm, 314.2 nm, 337 nm, 355.9 nm, 374.1 nm, 378.9 nm, 387.9 nm, 398.4 nm, and 404.7 nm), and N_2^+ (352.5 nm and 391 nm) lines [36–39] are quite consistent with the ion nitriding processes using H_2/N_2 mixture gases and NH_3 gas [8]. The major peak around 336 nm is the overlapping peaks of both NH emission and N_2 emission. For elucidating the nitriding mechanism in our APPN system, the generated plasma species of N_2^+, N_2, NH, N, and N^- were evidently ion-nitrided with the SKD11 sample to produce a plasma-induced hard nitride layer within 10 min. Once the treated process reached the end of the experiment, pure nitrogen gas was used to cool down the sample to room temperature to prevent possible oxidation. The entire process was completed in approximately 18 min.
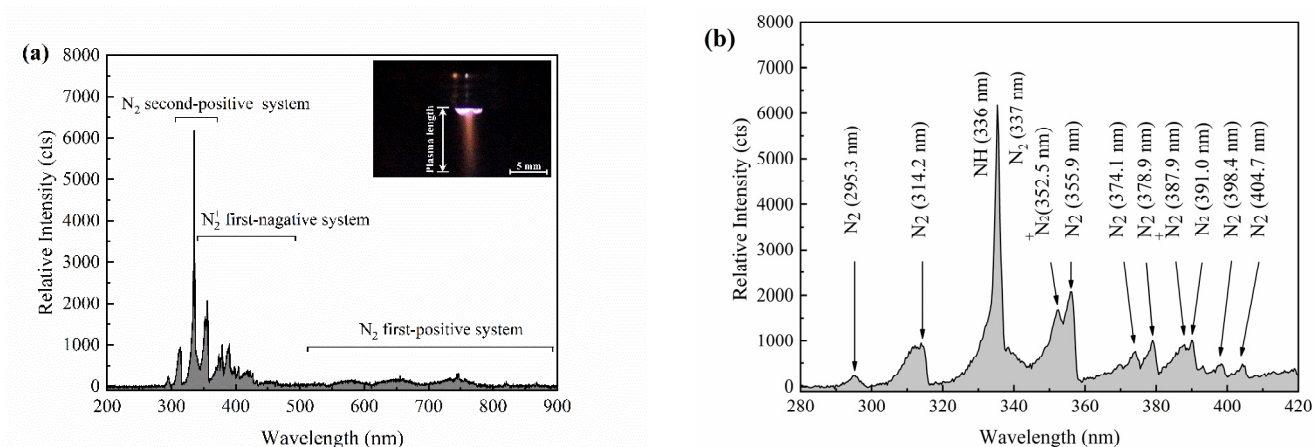

Figure 6. The measured optical emission spectra of H_2/N_2 plasma in an APPJ system: (**a**) full range from the wavelength of 200 to 900 nm, and (**b**) short range from 280 to 420 nm.

According to the results mentioned above for the experiments, surface treatment with H_2/N_2 plasma was achieved to produce the nitriding layer on SKD11 steel. In Figure 7, nitrogen and hydrogen mixture gas are passed into the nozzle to generate the plasma, in which the radicals of N, H, and NH are generated by electron collisions [40]. It has been reported in the literature that NH radicals play a key role in the nitriding process to promote the nitrogen atom diffusing into the steel and the nitriding layer formed on the steel surface [30,41,42]. In addition, the H_2/N_2 plasma discharges in the APPJ system create a high flux and a high density of reactive plasma species to bombard on the substrate

surface [43]. On the other hand, the quartz tube covered on the plasma jet was observed to possess the heat preservation. As a result, the rapid rise of substrate temperature in a short time during the APPN process achieved a rapid nitriding on the samples.
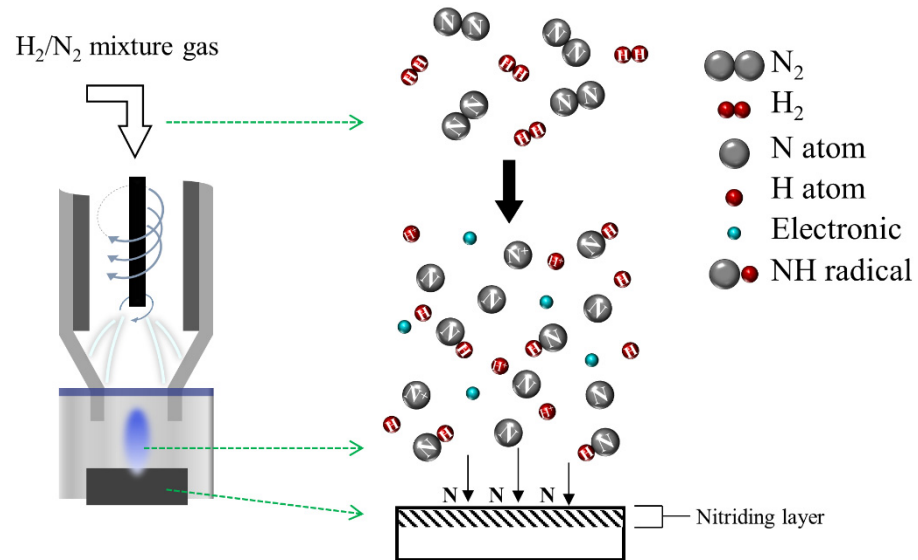

Figure 7. Nitriding formation mechanism on SKD11 cold-work steel sample by APPN.

The hardening treatment on SKD11 cold-work tool steel for improving its wear resistance traditionally applies the ion nitriding process in a vacuum system. It utilizes the operating conditions of a low nitriding pressure, a temperature ranging from 400 to 600 °C, and quite a long duration (typically 3–80 h). The APPN process offers high flux density of nitriding plasma species and a rapid thermal nitriding process without any vacuum systems involved, which can be used to alter the mechanical properties of metal substrates.

The mechanical properties of the pristine and APPN-treated SKD11 samples were experimentally measured by using the nanoindentation test. A schematic illustration of the continuous load versus displacement curves (P–h) of the samples is presented in Figure 8. The indentation load of maximum (P_{max}) is 5000 µN and the P–h curves with the loading and unloading processes were observed. Compared with the base material, the maximum indentation displacement (h_{max}) of the APPN-treated sample decreased from 128 to 117 nm. In Figure 9a, the hardness and reduced Young's modulus values of pristine SKD11 were 7.35 ± 0.54 GPa and 186.50 ± 7.02 GPa, respectively. The APPN-treated samples significantly increased to the values of 10.94 ± 0.89 GPa and 218.32 ± 7.67 GPa.

In this study, ν_s is the Poisson's ratio of SKD11 cold-work steel [44,45]. The values of Young's modulus (E) were accordingly calculated from Equation (1). As compared with the pristine SKD11, the increase in the E value of APPN-treated samples was 242.15 ± 10.55 GPa. Therefore, in Figure 9b, we display the combined plot of the different calculation data based on the ratios of hardness and elastic modulus, such as H/E and H^3/E^2, referring to the indication of material's deformation resistance [46,47]. The first ratio, H/E, represents the resistance of the material to elastic strain failure. The second ratio, H^3/E^2, is commonly used to describe the plastic deformation resistance of the material. The values of H/E and H^3/E^2 of the APPN-treated SKD11 (4.514×10^{-2} and 2.244×10^{-2}) increased as compared to those of the base material (3.629×10^{-2} and 9.799×10^{-3}), indicating that higher wear resistance of the nitrided layer induced by an APPN process on the samples' surface was feasibly achieved.

The higher ratios of hardness and elastic modulus are also in general correlated with the resistance toward impacts and plastic deformation. We utilized the impact wear testing with repeated collisions of a ball indenter to observe the cracks and eventual damage on the surface of the prepared samples [10,11,20]. In Figure 10a, the pristine SKD11 sample displayed a circle shape with a width of 311.2 µm and depth of 5.3 µm for the impact

crater on the substrate for 10^5 cycles, as well as obvious cracks on the edge of the crater. The surface oxidation analyzed by EDS oxygen elemental mapping might be due to the oxidation thermally induced by the high-speed impact.
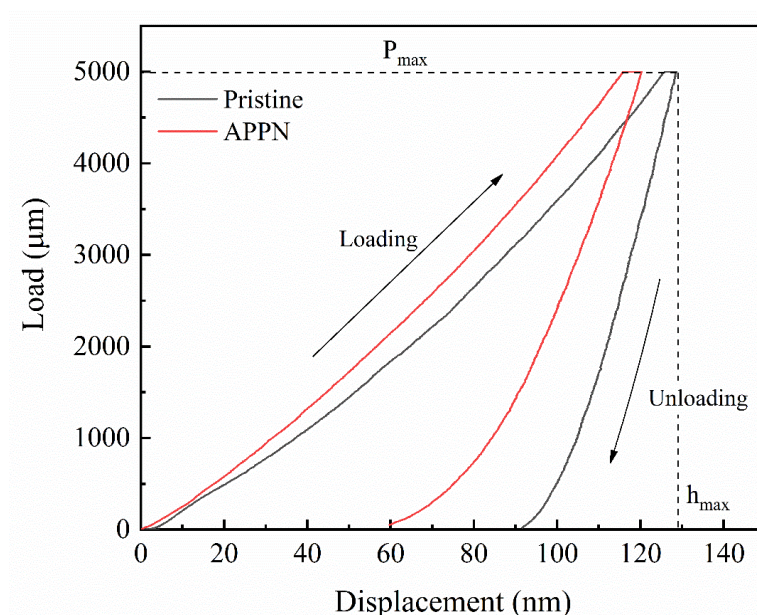

Figure 8. Nanoindentation load-displacement curves for pristine and APPN-treated SKD11 samples.
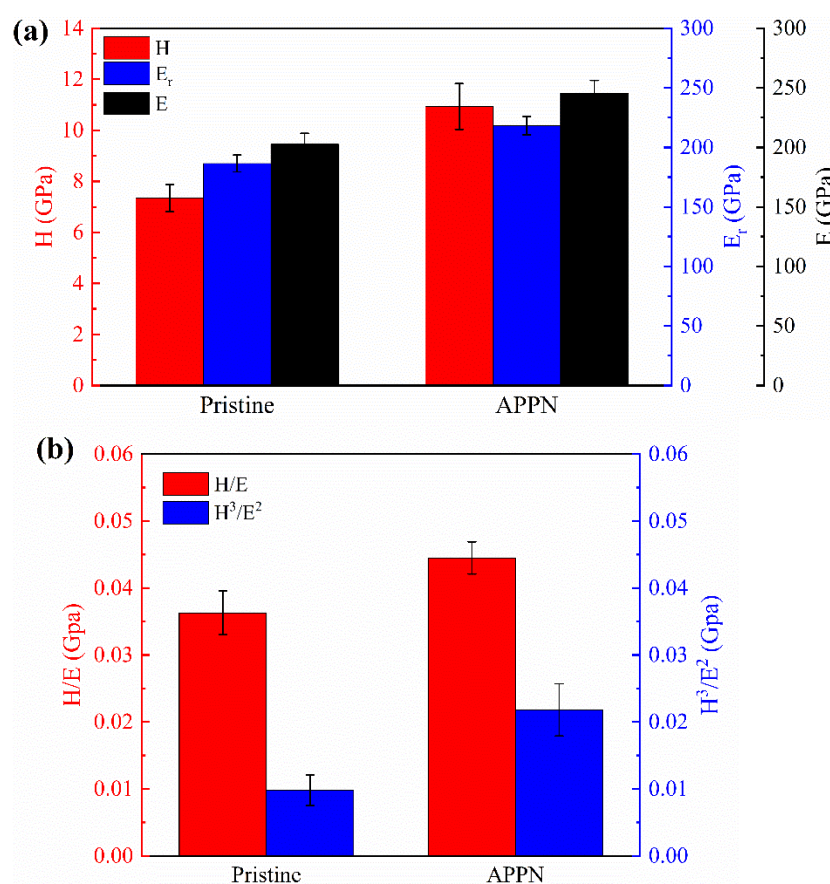

Figure 9. Illustrations of the variation of: (**a**) H, E_r, and E; and (**b**) calculated ratios of H/E and H^3/E^2 of pristine and APPN-treated SKD11 samples.
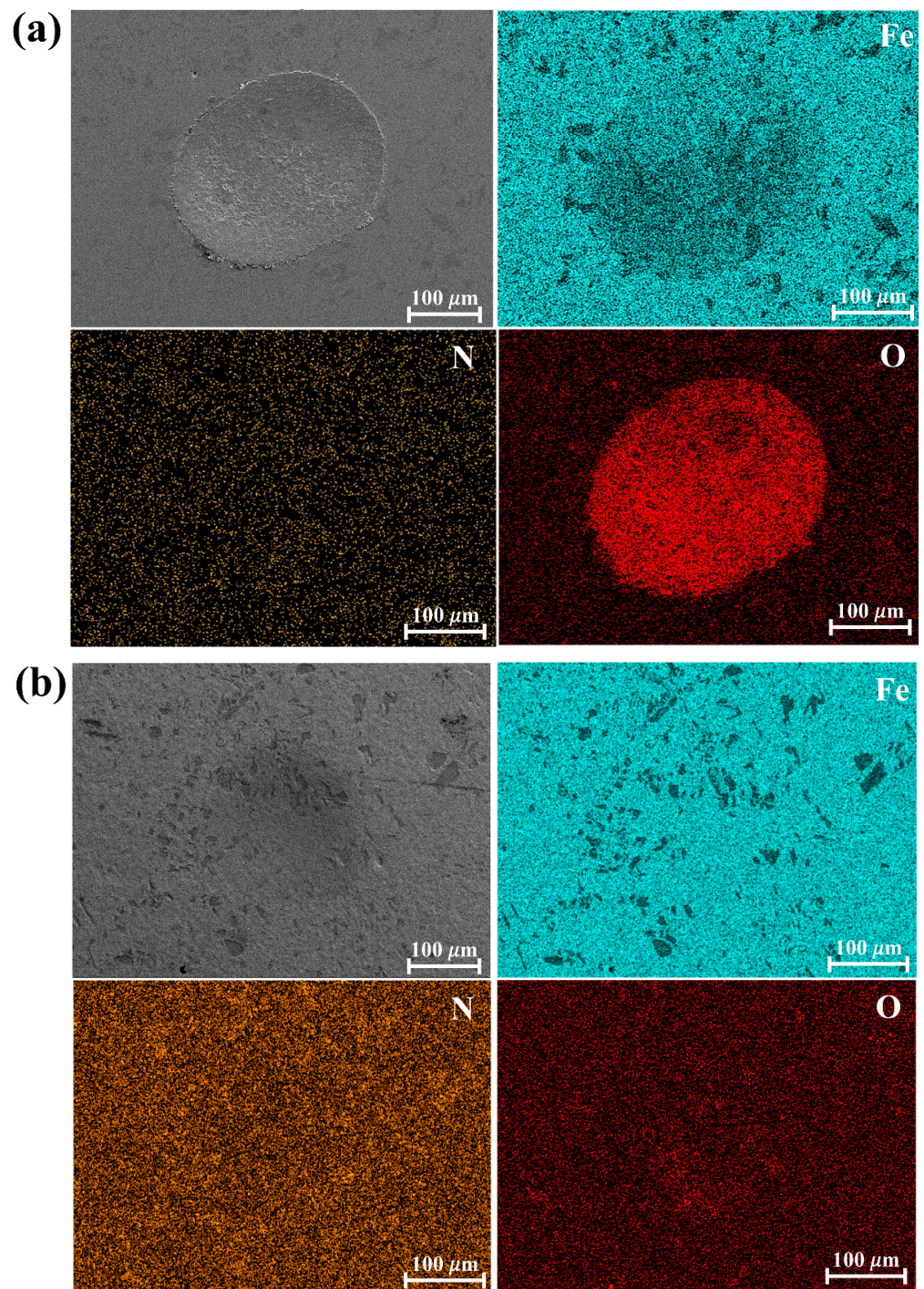
Figure 10. Crater photos and SEM-EDS elemental mapping images of samples after 10^5 cycling impact wear tests: (**a**) pristine SKD11 and (**b**) APPN-treated SKD11.

In Figure 10b, the APPN-treated SKD11 sample showed a smaller width of 233.2 μm and a lower depth of 3.4 μm for the crater, with less oxidation on the surface. When increasing the cycling numbers of impacts on the samples, the APPN-treated samples were proven to have higher impact wear resistance, as displayed in Figure 11a,b. Yilmaz et al. reported that more multi-cycling impacts simultaneously resulted in the width and depth of craters, which was demonstrated to propose the wear mechanism that occurred in the form of delamination and flake-like spalling [11]. Interestingly, the depths of the craters are

obtained within the compound layer, and the EDS nitrogen elemental mapping showed the uniform distribution of the nitrogen signal.
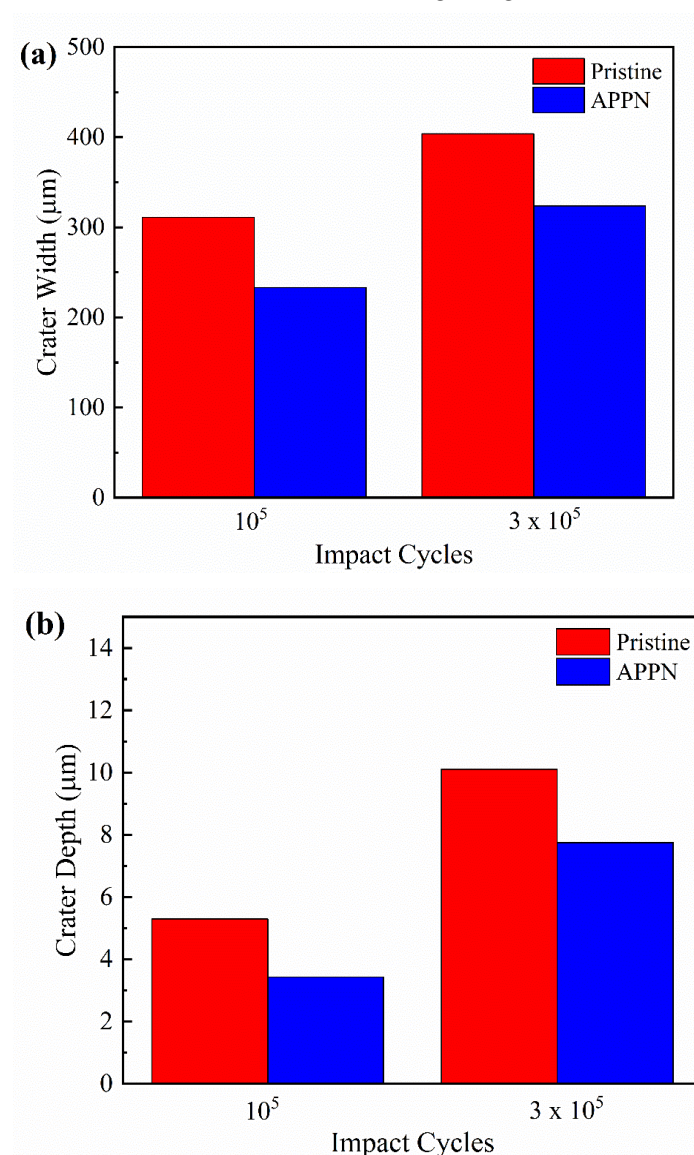

Figure 11. (**a**) Width and (**b**) depth of craters of pristine and APPN-treated SKD11 samples after 10^5 and 3×10^5 cycling impact wear tests.

The results of the hardness–elastic modulus ratios and impact wear testing indicate that the plasma-nitrided hard layer minimizes plastic deformation, which improves the life-time of SKD11 as die materials. So far, the kinetics of the nitriding process, which explores the diffusion behavior of nitrogen in solids, mainly relate to the process parameters (substrate temperature, nitriding time, and operating pressure) and the substrate conditions. We believe that tunable hardness of the APPN-induced hard layer on SKD11 used in die industries can be achieved by altering the process parameters in an APPJ system, such as the effects of the flow ratio of H_2/N_2 gas mixture, AC power supply, working distance, and treated time.

4. Conclusions

In summary, we utilized an atmospheric pressure plasma jet by using a H_2/N_2 gas mixture to thermally grow the nitride layer on SKD11 for improving its impact wear behavior. The generated reactive nitrogen-related plasma species and the plasma-induced heat accumulated on the substrate offer rapid ion-bombardment energy for the diffusion

of nitrogen species into the matrix for the nitriding process. The APPN-treated SKD11 substrate produced a nitride layer and diffusion layer with a total thickness of 44 μm above the matrix within 18 min. As formed on the SKD11 substrate, the nitride hard layer presented an improved surface hardness (1095 ± 15.5 HV$_{0.3}$), while the values in the diffusion zone decreased dramatically due to the nitrogen dissolution profile inside the iron lattice. The nanohardness and Young's modulus of APPN-treated SKD11 increased by 44.9% and 19.4% compared with the pristine specimens, respectively. The increases in the ratios of the hardness–elastic modulus were distinctly obtained, indicating a higher deformation resistance of the nitrided layer on the SKD11 surface. As multi-cycling impact tests were applied, the surface on the formed nitride hard layer displayed smaller and shallower impact craters, which could correlate to minimization of the plastic deformation occurring. The results of indentation and impact wear showed that the protective coating on the APPN-treated specimen had better mechanical properties. The APPN process has the potential to become a rapid thermal nitriding technology for offering high flux and high density of nitriding plasma species on SKD11 for improving its lifetime when used as die materials. We also note that this thermochemical process can likewise be employed for the tunable hardness of steel in die industries.

References

1. Groover, M.P. *Fundamentals of Modern Manufacturing: Materials, Processes, and Systems*, 4th ed.; John Wiley & Sons: Hoboken, NJ, USA, 2020; pp. 99–136.
2. Koshy, P.; Dewes, R.C.; Aspinwall, D.K. High speed end milling of hardened AISI D2 tool steel ($\sim$ to 58 HRC). *J. Mater. Process Technol.* **2002**, *127*, 266–273. [CrossRef]
3. Tucker, R.C. *ASM Handbook, Volume 5A: Thermal Spray Technology*; ASM International: Materials Park, OH, USA, 2013; pp. 14–35.
4. Wen, D.C. Plasma nitriding of plastic mold steel to increase wear and corrosion properties. *Surf. Coat. Technol.* **2009**, *204*, 511–519. [CrossRef]
5. Zagonel, L.F.; Figueroa, C.A.; Droppa, R., Jr.; Alvarez, F. Influence of the process temperature on the steel microstructure and hardening in pulsed plasma nitriding. *Surf. Coat. Technol.* **2006**, *201*, 452–457. [CrossRef]
6. Yamagata, H. *The Science and Technology of Materials in Automotive Engines*, 1st ed.; Elsevier: Amsterdam, The Netherlands, 2005; pp. 165–204.
7. Schaaf, P.; Kasper, J.; Höche, D. Laser gas assisted nitriding of Ti alloys. In *Comprehensive Materials Processing-Laser Machining and Surface Treatment*; Hashmi, S., Batalha, G.F., VanTyne, C.J., Yilbas, B., Eds.; Elsevier: Amsterdam, The Netherlands, 2014; Volume 9, pp. 261–278.
8. Aghajani, H.; Behrangi, S. *Plasma Nitriding of Steels*, 1st ed.; Springer International Publishing: Cham, Switzerland, 2017; pp. 1–67.
9. Chandler, H. *Heat Treater's Guide: Practices and Procedures for Irons and Steels*, 2nd ed.; ASM International: Materials Park, OH, USA, 1994; pp. 27–77.

10. Zhao, C.; Zha, W.; Zhang, J.; Nie, X. Surface fatigue cracking of plasma nitrided cast iron D6510 under cyclic inclined contact stresses. *Int. J. Fatigue.* **2019**, *124*, 10–14. [CrossRef]

11. Yilmaz, H.; Sadeler, R. Impact wear behavior of ball burnished 316L stainless steel. *Surf. Coat. Technol.* **2019**, *363*, 369–378. [CrossRef]

12. Ko, C.L.; Kuo, Y.L.; Lee, W.J.; Sheng, H.J.; Guo, J.Y. The enhanced abrasion resistance of an anti-fingerprint coating on chrome-plated brass substrate by integrating sputtering and atmospheric pressure plasma jet technologies. *Appl. Surf. Sci.* **2018**, *448*, 88–94. [CrossRef]

13. Michael, F.M.; Khalid, M.; Walvekar, R.; Siddiqui, H.; Balaji, A.B. Surface modification techniques of biodegradable and biocompatible polymers. In *Biodegradable and Biocompatible Polymer Composites: Processing, Properties and Applications*; Shimpi, N.G., Ed.; Woodhead Publishing: Sawston, UK, 2018; pp. 33–54.

14. Miyamoto, J.; Inoue, T.; Tokuno, K.; Tsutamori, H.; Abraha, P. Surface modification of tool steel by atmospheric-pressure plasma nitriding using dielectric barrier discharge. *Tribol. Online* **2016**, *11*, 460–465. [CrossRef]

15. Sato, S.; Arai, Y.; Yamashita, N.; Kojyo, A.; Kodama, K.; Ohtsu, N.; Okamoto, Y.; Wagatsuma, K. Surface-nitriding treatment of steels using microwave-induced nitrogen plasma at atmospheric pressure. *Appl. Surf. Sci.* **2012**, *258*, 7574–7580. [CrossRef]

16. Nagamatsu, H.; Ichiki, R.; Yasumatsu, Y.; Inoue, T.; Yoshida, M.; Akamine, S.; Kanazawa, S. Steel nitriding by atmospheric-pressure plasma jet using N2/H2 mixture gas. *Surf. Coat. Technol.* **2013**, *225*, 26–33. [CrossRef]

17. Patnaik, P. *A comprehensive Guide to the Hazardous Properties of Chemical Substances*, 3rd ed.; John Wiley & Sons: Hoboken, NJ, USA, 2007; pp. 402–410.

18. Kajdas, C.; Wilusz, E.; Harvey, S. *Encyclopedia of Tribology*, 1st ed.; Elsevier: Amsterdam, The Netherlands, 1990; pp. 2420–2424.

19. Oliver, W.C.; Pharr, G.M. An improved technique for determining hardness and elastic modulus using load and displacement sensing indentation experiments. *J. Mater. Res.* **1992**, *7*, 1564–1583. [CrossRef]

20. Knotek, O.; Bosserhoff, B.; Schrey, A.; Leyendecker, T.; Lemmer, O.; Esser, S. A new technique for testing the impact load of thin films: The coating impact test. *Surf. Coat. Technol.* **1992**, *54*, 102–107. [CrossRef]

21. Jcpds Card No: 65-7296. International Centre for Diffraction Data. Available online: https://www.icdd.com/ (accessed on 1 August 2021).

22. Jcpds Card No: 88-2323. International Centre for Diffraction Data. Available online: https://www.icdd.com/ (accessed on 1 August 2021).

23. Jcpds Card No: 22-0211. International Centre for Diffraction Data. Available online: https://www.icdd.com/ (accessed on 1 August 2021).

24. Jcpds Card No: 06-0091. International Centre for Diffraction Data. Available online: https://www.icdd.com/ (accessed on 1 August 2021).

25. Jcpds Card No: 77-2006. International Centre for Diffraction Data. Available online: https://www.icdd.com/ (accessed on 1 August 2021).

26. Jcpds Card No: 11-0065. International Centre for Diffraction Data. Available online: https://www.icdd.com/ (accessed on 1 August 2021).

27. Díaz-Guillén, J.C.; Díaz-Guillén, J.A.; Granda-Gutiérrez, E.E.; Díaz-Guillén, M.R.; González-Albarrán, M.A. Electrochemical corrosion performance of AISI D2 tool steel surface hardened by pulsed plasma nitriding. *Int. J. Electrochem. Sci.* **2013**, *8*, 973–982.

28. Conci, M.D.; Bozzi, A.C.; Franco Jr, A.R. Effect of plasma nitriding potential on tribological behaviour of AISI D2 cold-worked tool steel. *Wear* **2014**, *317*, 188–193. [CrossRef]

29. Chastain, J.; King, R.C., Jr. *Handbook of X-ray Photoelectron Spectroscopy*, 1st ed.; Perkin-Elmer: Eden Prairie, MN, USA, 1992; pp. 40–86.

30. Moskalioviene, T.; Galdikas, A. The effect of hydrogen on plasma nitriding of austenitic stainless steel: Kinetic modeling. *Met. Mater. Trans. A* **2015**, *46*, 5588–5595. [CrossRef]

31. Naeem, M.; Iqbal, J.; Abrar, M.; Khan, K.H.; Díaz-Guillén, J.C.; Lopez-Badillo, C.M.; Shafiq, M.; Zaka-ul-Islam, M.; Zakaullah, M. The effect of argon admixing on nitriding of plain carbon steel in N2 and N2-H2 plasma. *Surf. Coat. Technol.* **2018**, *350*, 48–56. [CrossRef]

32. Dunlap, R.A. The symmetry and packing fraction of the body centered tetragonal structure. *Eur. J. Phys.* **2017**, *3*, 17–24.

33. Bhadeshia, H.; Honeycombe, R. *Steels: Microstructure and Properties*, 4th ed.; Butterworth-Heinemann Elsevier Ltd.: Oxford, UK, 2017; pp. 1–30.

34. Pye, D. *Practical Nitriding and Ferritic Nitrocarburizing*, 1st ed.; ASM International: Materials Park, OH, USA, 2003; pp. 1–37.

35. NIST Atomic Spectra Database. Available online: https://www.nist.gov/pml/atomic-spectra-database (accessed on 12 May 2014).

36. Brühl, S.; Russell, M.; Gómez, B.; Grigioni, G.; Feugeas, J.; Ricard, A. A study by emission spectroscopy of the N2 active species in pulsed dc discharges. *J. Phys. D Appl. Phys.* **1997**, *30*, 2917–2922. [CrossRef]

37. Lamichhane, P.; Ghimire, B.; Mumtaz, S.; Paneru, R.; Ki, S.H.; Choi, E.H. Control of hydrogen peroxide production in plasma activated water by utilizing nitrification. *J. Phys. D Appl. Phys.* **2019**, *52*, 26520601–26520609. [CrossRef]

38. Corujeira Gallo, S.; Charitidis, C.; Dong, H. Surface functionalization of carbon fibers with active screen plasma. *J. Vac. Sci. Technol. A.* **2017**, *35*, 021404. [CrossRef]

39. Hsu, C.C.; Yang, Y.J. The increase of the jet size of an atmospheric-pressure plasma jet by ambient air control. *IEEE Trans. Plasma Sci.* **2010**, *38*, 496–499. [CrossRef]

40. Petitjean, L.; Ricard, A. Emission spectroscopy study of N2-H2 glow discharge for metal surface nitriding. *J. Phys. D Appl. Phys.* **1984**, *17*, 919. [CrossRef]
41. Priest, J.M.; Baldwin, M.J.; Fewell, M.P. The action of hydrogen in low-pressure rf-plasma nitriding. *Surf. Coat. Technol.* **2001**, *145*, 152–163. [CrossRef]
42. Martinez, H.; Yousif, F.B. Electrical and optical characterization of pulsed plasma of N2-H2. *Eur. Phys. J. D* **2008**, *46*, 493–498. [CrossRef]
43. Selwyn, G.S.; Herrmann, H.W.; Park, J.; Henins, I. Materials processing using an atmospheric pressure, rf-generated plasma source. *Contrib. Plasma Phys.* **2001**, *41*, 610–619. [CrossRef]
44. Zheng, Q.; Shimizu, T.; Yang, M. Finite element analysis of springback behavior in resistance heating assisted microbending process. *Mech. Eng. J.* **2015**, *2*, 14-00413–14-00414. [CrossRef]
45. Chen, J.S.; Yu, C.; Lu, H. Phase stability, magnetism, elastic properties and hardness of binary iron nitrides from first principles. *J. Alloy Compd.* **2015**, *625*, 224–230. [CrossRef]
46. Santos, E., Jr.; Nascimento, K.D.; Camargo, S.S., Jr. Relation between in-vitro wear and nanomechanical properties of commercial light-cured dental composites coated with surface sealants. *Mat. Res.* **2013**, *16*, 1148–1155. [CrossRef]
47. Tsui, T.; Pharr, G.; Oliver, W.; Bhatia, C.; White, R.; Anders, S.; Anders, A.; Brown, I. Nanoindentation and nanoscratching of hard carbon coatings for magnetic disks. *Mater. Res. Soc. Symp. Proc.* **1995**, *383*, 447–452. [CrossRef]